Inorg. Chem. **2007**, *46*, 5528–5536

Toward Actinide Molecular Magnetic Materials: Coordination Polymers of U(IV) and the Organic Acceptors TCNQ and TCNE†

Eric J. Schelter,* David E. Morris, Brian L. Scott, Joe D. Thompson, and Jaqueline L. Kiplinger*

Los Alamos National Laboratory, Los Alamos, New Mexico 87545

Received January 8, 2007

Molecular materials of transition metal ions and organic acceptors of the general formula $M(TCNX)_2$ M = V, Mn, Fe, Co, Ni; X = Q = 7,7,8,8-tetracyano-*p*-quinodimethane, E = tetracyanoethylene, are known to exhibit magnetic ordering resulting from magnetic interactions between the 3d metal orbitals of the paramagnetic metal ion and π^* orbitals of the organic radical spin centers. The reaction of THF solutions of $UI_3(THF)_4$ with neutral TCNQ and TCNE instantaneously produce insoluble coordination polymers that can be assigned a formula of $[U(TCNX)_2I_2(THF)_2]_n$ on the basis of elemental analysis. Similar reactions between (K-18-crown-6)(TCNX) reagents and $UI_3(THF)_4$ produce materials with slightly different phase compositions that are structurally distinct from the neutral TCNQ and TCNE reaction products, as judged by infrared spectroscopy. In all cases the magnetic response of these materials is consistent with the presence of the U(IV) rather than U(III) ion. Voltammetric data obtained for all the synthetic precursors are consistent with the U(IV)/TCNX radical anion formulation. None of the materials undergo magnetic ordering, presumably due to the singlet magnetic ground state that results from the U(IV) ion in a low-symmetry ligand field.

Introduction

Magnetic coordination polymers containing paramagnetic metal ions linked by organic radicals through coordination bonds represent one of the cornerstones of modern magneto chemistry.[1−9] Such materials often exhibit magnetic ordering, even above room temperature, as a result of strong antiferromagnetic coupling between spins located in the metal d- or f-orbitals and organic radical π^* orbitals. The most extensive studies of these materials have been performed with divalent 3d transition metal ions and 7,7,8,8-tetracyano-*p*-quinonedimethane (TCNQ) or tetracyanoethylene (TCNE), which form stable one-electron organic radicals at a potential of −0.33 and −0.35 V, respectively, in THF at a Pt working electrode versus $Fc^{+/0}$ (Figure 1). Metal−TCNX materials are typically prepared by reduction of the organic group by low-valent metal ion precursors,[10,11] or by reacting salts of the organic radicals with metal coordination complexes containing good leaving groups.[2,7,12,13] The insolubility, structural complexity, and potential for polymorphism of these materials often prevent the growth of large single crystals for analysis, but the $\nu_{C\equiv N}$, $\nu_{C=C}$, and $\nu_{C-H(bend)}$ vibrational modes of the organic radicals provide excellent spectroscopic markers to monitor their reduction and coordination mode.[14,15]

Lanthanide ions form similar types of coordination polymers with TCNQ and TCNE and, in the case of Dy(III) and Gd(III), exhibit magnetic ordering at low temperatures.[12,16] The observed ordering in these materials is interesting, as

† This paper is dedicated to the memory of Dr. Mervin J. Bazile, Jr. (1977-2005).

* To whom correspondence should be addressed. Fax: +01 505 667 9905 (E.J.S.). Tel: +01 505 665 9553 (E.J.S.). E-mail: schelter@lanl.gov (E.J.S.).

(1) Miller, J. S. *Inorg. Chem.* **2000**, *39*, 4392.
(2) O'Kane, S. A.; Clerac, R.; Zhao, H. H.; Xiang, O. Y.; Galan-Mascaros, J. R.; Heintz, R.; Dunbar, K. R. *J. Solid State Chem.* **2000**, *152*, 159.
(3) Kahn, M. L.; Sutter, J. P.; Golhen, S.; Guionneau, P.; Ouahab, L.; Kahn, O.; Chasseau, D. *J. Am. Chem. Soc.* **2000**, *122*, 9566.
(4) Miller, J. S.; Epstein, A. J. *Coord. Chem. Rev.* **2000**, *206*, 651.
(5) Miller, J. S.; Benelli, C.; Gatteschi, D. *Chem. Rev.* **2002**, *102*, 2369.
(6) Miller, J. S. *Adv. Mater.* **2002**, *14*, 1105.
(7) Clerac, R.; O'Kane, S.; Cowen, J.; Ouyang, X.; Heintz, R.; Zhao, H.; Bazile, M. J., Jr.; Dunbar, K. R. *Chem. Mater.* **2003**, *15*, 1840.
(8) Koivisto, B. D.; Hicks, R. G. *Coord. Chem. Rev.* **2005**, *249*, 2612.
(9) Miller, J. S. *Dalton Trans.* **2006**, 2742.
(10) Manriquez, J. M.; Yee, G. T.; McLean, R. S.; Epstein, A. J.; Miller, J. S. *Science* **1991**, *252*, 1415.
(11) Vickers, E. B.; Senesi, A.; Miller, J. S. *Inorg. Chim. Acta* **2004**, *357*, 3889.
(12) Zhao, H.; Bazile, M. J., Jr.; Galan-Mascaros, J. R.; Dunbar, K. R. *Angew. Chem., Int. Ed.* **2003**, *42*, 1015.
(13) Vickers, E. B.; Giles, I. D.; Miller, J. S. *Chem. Mater.* **2005**, *17*, 1667.
(14) Miller, J. S. *Angew. Chem., Int. Ed.* **2006**, *45*, 2508.
(15) Kaim, W.; Moscherosch, M. *Coord. Chem. Rev.* **1994**, *129*, 157.
(16) Raebiger, J. W.; Miller, J. S. *Inorg. Chem.* **2002**, *41*, 3308.

10.1021/ic0700295 CCC: $37.00
Published on Web 06/15/2007

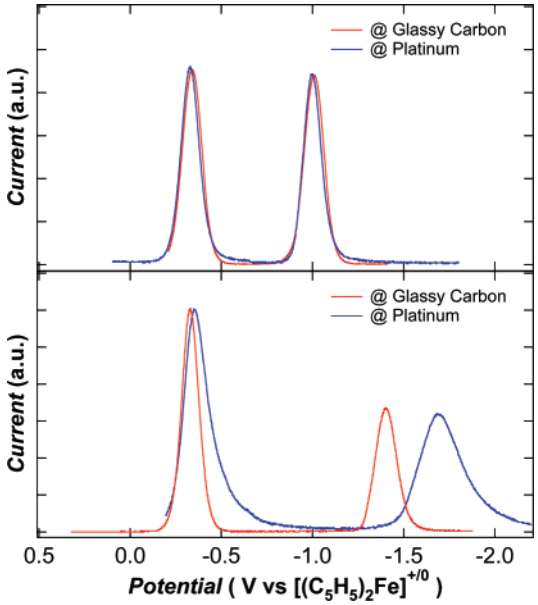

Figure 1. Square-wave voltammograms of TCNQ (top) and TCNE (bottom) in ~0.1 M $[Bu_4N][B(C_6F_5)_4]$/THF at working electrode indicated.

lanthanide ions form essentially ionic complexes due to the corelike 4f orbitals that are unable to overlap effectively with ligand orbitals. Contrary to lanthanide systems, the 5f and 6d orbitals of the light actinides are much less contracted,[17] and there are certain classes of compounds where the 5f orbitals have been shown to play a significant role in covalent metal−ligand bonding.[18−21] On the basis of these observations, we were interested in preparing uranium organic-radical materials. Signatures of covalency in actinide systems have been studied by us and others and should result in stronger magnetic exchange interactions compared to lanthanide systems. Specifically, the mean field description of magnetic ordering predicts higher ordering temperatures (T_c) for stronger magnetic exchange interactions (J) and greater number of nearest-neighbor spin centers (z) where $T_c = 2JzJ(J+1)/3k_B$; k_B = Boltzmann's constant.[16] As such, tri- and tetravalent actinides are predicted to exhibit higher ordering temperatures than their lanthanide−TCNX counterparts. Comparison of actinide−, lanthanide−, and transition metal−TCNX material ordering temperatures will provide an unambiguous report on the relative strength of magnetic coupling between these materials.

Building on our previous work using nitrile-based ligands to prepare uranium(IV) and thorium(IV) complexes that show spectroscopic signatures of covalent metal−ligand interactions,[18,22] we now report on the reaction of $UI_3(THF)_4$ with neutral and reduced TCNQ and TCNE[23] and the magnetic properties of the resulting coordination polymers.

Experimental Section

Unless otherwise noted, reactions and manipulations were performed at ambient temperature in a recirculating Vacuum Atmospheres Model HE-553-2 inert-atmosphere (N_2) drybox equipped with a MO-40-2 Dri-Train or in a fume hood using standard Schlenk and high-vacuum line techniques. Glassware was dried overnight at 150 °C before use. Elemental analyses were performed at the University of California, Berkeley Microanalytical Facility, on a Perkin-Elmer Series II 2400 CHNS analyzer. The starting material $UI_3(THF)_4$ was prepared according to a modified literature procedure.[24] ***Caution:*** *Depleted uranium (primarily isotope ^{238}U) is a weak α-emitter with a half-life of 4.47×10^9 years; manipulations and reactions should be carried out in monitored fume hoods or in an inert-atmosphere drybox in a radiation laboratory equipped with α- and β-counting equipment.* Potassium metal, TCNQ, and TCNE (Aldrich) were used without further purification. THF (Aldrich) was dried by passage through a double-column system of alumina (A2, 12 × 32, Purifry) under nitrogen pressure, stored over activated 4 Å molecular sieves, and tested with Na/benzophenone-ketyl prior to use. 18-Crown-6 (Aldrich) was recrystallized from hot acetonitrile and dried under dynamic vacuum before use.

Voltammetric data were obtained in the inert-atmosphere drybox described above. All data were collected using a Perkin-Elmer Princeton Applied Research Corporation (PARC) Model 263 potentiostat under computer control with PARC Model 270 software. All sample solutions were ~1−5 mM in complex with 0.1 M $[Bu_4N][B(C_6F_5)_4]$ supporting electrolyte in THF solvent. All data were collected with the positive-feedback IR compensation feature of the software/potentiostat activated to minimize contribution to the voltammetric waves from uncompensated solution resistance (typically ~1 kΩ under the conditions employed). Solutions were contained in PARC Model K0264 microcells consisting of a ~3 mm diameter Pt or glassy carbon disk working electrode, a Pt wire counter electrode, and a silver wire quasi-reference electrode. Scan rates from 20 to 5000 mV/s were employed to assess the chemical and electrochemical reversibility of the observed redox transformations. Potential calibrations were performed at the end of each data collection cycle using the ferrocenium/ferrocene ($Fc^{+/0}$) couple as an internal standard.

DC magnetic measurements at $H = 5$ T over the temperature range 2−350 K (cooled in zero field to 2 K with measurement on warming) and AC measurements at $H = 0$ T from 100 to 2 K were made using a Quantum Design superconducting quantum interference device (SQUID) magnetometer. The samples were sealed in 5 mm Wilmad 505-PS borosilicate NMR tubes along with a small amount of quartz wool to hold the sample in place. Contributions to the magnetization from the quartz wool and tube were measured independently and subtracted from the total measured signal. Diamagnetic corrections were made using Pascal's constants.

Infrared spectra were recorded on a Thermo Electron Nicolet Avatar DTGS FT-IR spectrometer at 1 cm^{-1} resolution as mineral oil mulls suspended between KBr plates. Both magnetic and infrared spectroscopy samples were prepared in the inert-atmosphere drybox described above.

(17) Morss, L. R.; Edelstein, N. M.; Fuger, J. *The Chemistry of the Actinide and Transactinide Elements*, 3rd ed.; Springer: Dordrecht, 2006; Vol. 3, p 2111.
(18) Morris, D. E.; Da Re, R. E.; Jantunen, K. C.; Castro-Rodriguez, I.; Kiplinger, J. L. *Organometallics* **2004**, *23*, 5142 and references cited therein.
(19) Ephritikhine, M. *Dalton Trans.* **2006**, 2501.
(20) Diaconescu, P. L.; Cummins, C. C. *J. Am. Chem. Soc.* **2002**, *124*, 7660.
(21) Evans, W. J.; Kozimor, S. A.; Ziller, J. W. *Science* **2005**, *309*, 1835.
(22) Schelter, E. J.; Veauthier, J. M.; Thompson, J. D.; Scott, B. L.; John, K. D.; Morris, D. E.; Kiplinger, J. L. *J. Am. Chem. Soc.* **2006**, *128*, 2198.
(23) Rossetto, G.; Brianese, N.; Ossola, F.; Porchia, M.; Zanella, P.; Sostero, S. *Inorg. Chim. Acta* **1987**, *132*, 275.
(24) Golden, J. T.; Jantunen, K. C.; Kiplinger, J. L.; Clark, D. L.; Burns, C. J.; Sattelberger, A. P. *Inorg. Synth.* **2006**, submitted.

X-ray crystallographic data were collected on a Bruker D8 diffractometer, with an APEX II charge-coupled-device (CCD) detector and a KRYO-FLEX liquid nitrogen vapor-cooling device.

$[U(TCNQ)_2I_2(THF)_2]_n$ (1). A 125 mL flask was charged with TCNQ (0.374 g, 1.83 mmol, 4 equiv) and 75 mL of THF. To this clear, green solution solid $UI_3(THF)_4$ (0.414 g, 0.456 mmol) was added with stirring. The mixture immediately changed color to dark green and a green precipitate appeared. The mixture was stirred for 14 h, and the resulting green suspension filtered over a medium-porosity frit to isolate crude **1** as a green solid. The solid was washed with THF (5 × 10 mL) until the washings were colorless and dried for 8 h under dynamic vacuum to give **1** as an analytically pure green solid (0.296 g, 0.283 mmol, 62%). Anal. Calcd for $C_{32}H_{24}I_2N_8O_2U$ (1044.42 g/mol): C, 36.80; H, 2.32; N, 10.73. Found: C, 36.68; H, 2.15; N, 10.53. IR (Nujol): $\nu_{C\equiv N}$ (cm^{-1}) 2188 s, 2091 s; $\nu_{C=C}$ 1506 s; $\nu_{C-H(bend)}$ 808 w, 824 w, 851 w.

$[U(TCNE)_2I_2(THF)_2]_n$ (2). A 125 mL flask was charged with TCNE (0.278 g, 2.17 mmol, 4 equiv) and 20 mL of THF. To this clear, yellow solution $UI_3(THF)_4$ (0.483 g, 0.532 mmol) was added with stirring. The mixture immediately changed color to brown and a reddish-brown precipitate appeared. The mixture was stirred for 72 h, and the resulting reddish-brown suspension filtered through a medium-porosity frit to collect crude **2** as a brown solid. The brown solid was washed with THF (5 × 2 mL) until the washings were colorless and dried for 4 h under dynamic vacuum to afford **2** as a light brown solid (0.183 g, 0.205 mmol, 42%). Anal. Calcd for $C_{20}H_{16}I_2N_8O_2U$ (892.23 g/mol): C, 26.92; H, 1.81; N, 12.56. Found: C, 26.94; H, 1.94; N, 11.40. IR (Nujol): $\nu_{C\equiv N}$ (cm^{-1}) 2187 s, 2149 sh, 2085 s.

[K-18-crown-6][TCNQ] (3). This material was prepared using a modification to the published literature procedure.[25] Freshly cut potassium metal (0.088 g, 2.25 mmol) was smeared on the bottom of a 125 mL flask, and 50 mL of THF was added. With stirring, TCNQ (0.460 g, 2.25 mmol) was added to this mixture, resulting in a clear, pale green solution. Immediately after addition of TCNQ, 18-crown-6 (0.610 g, 2.31 mmol) was added to the clear, green solution, which progressively turned darker green throughout the course of the reaction. After 36 h, the resulting dark green solution was filtered through a Celite-padded coarse frit. The filtrate was collected and the volume of the solution reduced to ~5−10 mL and then and placed in a −30 °C freezer. A dark blue crystalline solid formed, and the supernatant was decanted. The remaining crystals were washed with hexanes (3 × 5 mL) and dried under dynamic vacuum to give **3** (0.703 g, 1.39 mmol, 62%). The infrared spectrum of the product is consistent with reported values.[2,25] IR (Nujol): $\nu_{C\equiv N}$ (cm^{-1}) 2186 s, 2176 s, 2160 sh, 2155 s; $\nu_{C=C}$ (cm^{-1}) 1504 s; $\nu_{C-H(bend)}$ 833 m, 838 m, 843 sh.

[K-18-crown-6][TCNE] (4). Freshly cut potassium metal (0.095 g, 2.43 mmol) was smeared on the bottom of a 125 mL vacuum flask, and 50 mL of dry THF was added. With stirring, TCNE (0.312 g, 2.44 mmol) was added to this mixture, resulting in a clear, yellow solution. Immediately after addition of TCNE, 18-crown-6 (0.716 g, 2.71 mmol) was added to the yellow solution. After ~2 min, the solution turned orange and continued to darken throughout the course of the reaction. After 14 h, the resulting dark orange solution was filtered through a Celite-padded coarse frit. The filtrate was collected and the volatiles were removed under dynamic vacuum to give crude **4**. Recrystallization from hot THF (5 mL) afforded orange crystals of **4**. Further crystallization was accomplished by storing the solution overnight at −30 °C. The supernatant was decanted, and the orange crystalline solid was washed with hexanes (4 × 2 mL) and dried under dynamic vacuum to give analytically pure **4** (0.840 g, 1.95 mmol, 80%). Anal. Calcd for $C_{18}H_{24}KN_4O_6$ (431.51 g/mol): C, 50.10; H, 5.61; N, 12.98. Found: C, 50.47; H, 5.57; N, 13.02. IR (Nujol): $\nu_{C\equiv N}$ (cm^{-1}) 2191 s, 2153 s, 2140 sh.

$[U(TCNQ)_2I_2(THF)_{2.5}]_n$ (5). A 125 mL flask was charged with **3** (0.567 g, 1.12 mmol, 3 equiv) and THF (50 mL). To the resulting orange solution $UI_3(THF)_4$ (0.337 g, 0.372 mmol) was added with stirring. The mixture immediately changed color to dark green and a green precipitate appeared. The green suspension was stirred at room temperature for 14 h and filtered over a medium-porosity frit to collect a dark brown solid. The solid was washed with THF (6 × 10 mL) until the green washings were colorless and dried under dynamic vacuum for 8 h to give **5** as an analytically pure brown solid (0.233 g, 0.215 mmol, 58%). Anal. Calcd for $C_{34}H_{24}I_2N_8O_{2.5}U$ (1080.48 g/mol): C, 37.79; H, 2.61; N, 10.37. Found: C, 38.18; H, 2.75; N, 10.10. IR (Nujol): $\nu_{C\equiv N}$ (cm^{-1}) 2181 s, 2091 s; $\nu_{C=C}$ 1508 s; $\nu_{C-H(bend)}$ 824 m, 840 w.

$[U(TCNE)_2I_2(THF)_{1.5}]_n$ (6). A 125 mL flask was charged with **4** (0.539 g (1.25 mmol, 3 equiv) and THF (50 mL). To the resulting orange solution $UI_3(THF)_4$ (0.377 g, 0.416 mmol) was added with stirring. The solution darkened and changed color to brown. After 2 h the mixture had become a coffee brown suspension with a brown solid. The suspension was stirred for 16 h, and the solid collected by filtration over a medium-porosity frit, washed with THF (5 × 3 mL) until the orange-brown washings were colorless, and dried under dynamic vacuum for 8 h to give **6** as a brown solid (0.208 g, 0.243 mmol, 58%). Anal. Calcd for $C_{18}H_{12}I_2N_8O_{1.5}U$ (856.18 g/mol): C, 25.25; H, 1.41; N, 13.09. Found: C, 24.70; H, 2.04; N, 9.62. IR (Nujol): $\nu_{C\equiv N}$ (cm^{-1}) 2185 s, 2087 s.

Crystallographic Details for 4. An orange crystal (0.14 × 0.08 × 0.04 mm^3) grown from a concentrated acetonitrile solution of **4** at −30 °C was mounted in a nylon cryoloop using Paratone-N oil under argon gas flow. The instrument was equipped with graphite-monochromatized Mo Kα X-ray source (λ = 0.71073 Å) and MonoCap X-ray source optics. A hemisphere of data was collected using ω scans, with 5-s frame exposures and 0.3° frame widths. A total of 24 302 reflections ($-32 \le h \le 32$, $-14 \le k \le 14$, $-18 \le l \le 18$) was collected at T = 293(2) K in the θ range 1.52−25.37° of which 4499 were unique (R_{int} = 0.0962). Data collection and initial indexing and cell refinement were handled using APEX II software.[26] Frame integration, including Lorentz-polarization corrections, and final cell parameter calculations were carried out using SAINT+ software.[27] The data were corrected for absorption using a multiscan technique and the SADABS program.[28] Decay of reflection intensity was monitored by analysis of redundant frames. The structure was solved using direct methods and difference Fourier techniques. The TCNE molecules were disordered over two positions, and the central carbon atom positions, C(13) and C(14), were refined as two one-half occupancy positions. The cyanide groups of each TCNE component were refined in the same positions. All other hydrogen atoms were treated as idealized contributions. A disordered acetonitrile solvent molecule was treated with the SQUEEZE facility within the program PLATON (580 $Å^3$ and 171 electrons per unit cell).[29] The final refinement included anisotropic temperature factors on all non-hydrogen atoms. Structure

(25) Grossel, M. C.; Evans, F. A.; Hriljac, J. A.; Prout, K.; Weston, S. C. *J. Chem. Soc., Chem. Commun.* **1990**, 1494.

(26) *APEX II 1.08*; Bruker AXS Inc.: Madison, WI, 2004.
(27) *SAINT+ 7.06*; Bruker AXS, Inc.: Madison, WI, 2003.
(28) Sheldrick, G. *SADABS 2.03*; University of Göttingen: Göttingen, Germany, 2001.
(29) Spek, A. L. *Acta Crystallogr.* **1990**, *A46*, C34.

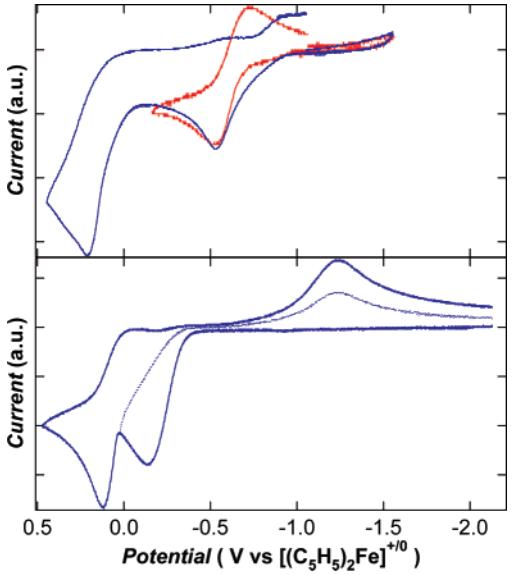

Figure 2. Cyclic voltammograms of $UI_3(THF)_4$ (top) and $[Bu_4N][I]$ (bottom) in ~0.1 M $[Bu_4N][B(C_6F_5)_4]$/THF at a glassy carbon working electrode.

solution, refinement, graphics, and creation of publication materials were performed using SHELXTL.[30]

Results and Discussion

Synthesis. Reaction of $UI_3(THF)_4$ with TCNQ and TCNE immediately produced insoluble **1** and **2**, which were isolated from their respective reaction mixtures by filtration (eq 1).

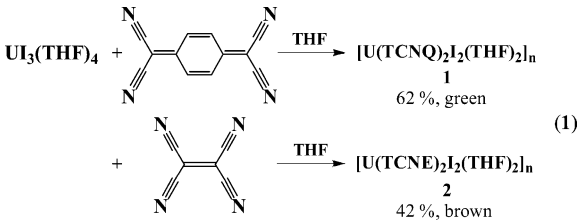

(1)

Efforts to grow single crystals of these materials, including slow exposure of reagent solutions, invariably produced powders.[12] In the course of the reactions, both the U(III) ion and iodide ligands provide reducing equivalents for the organic acceptors in the resulting coordination polymers. As shown in Figures 1 and 2, electron transfer from U(III) to the neutral electron acceptors is expected in these reactions on the basis of comparison of the U(IV)/U(III) (−0.62 V vs $Fc^{+/0}$) couple for $UI_3(THF)_4$ and reduction potentials of TCNQ and TCNE (−0.34 and −0.35 V, respectively) in THF (vide infra). Elemental analysis of **1** and **2** are consistent with two possible formulas for these materials. One possibility, $[U(TCNX)_2I_2(THF)_2]_n$, contains formally $TCNX^{\bullet-}$ ligands, while $[U(TCNX)_{1.5}I(THF)_{1.5}]_n$ includes $TCNX^{2-}$ to account for charge-balance considerations. As illustrated in Figure 3, the energies of the nitrile stretching bands for **1** and **2**, in comparison with reported $M(TCNX)_2$ materials, especially $V(TCNX)_2$,[10,31,32] support the presence of $TCNX^{\bullet-}$

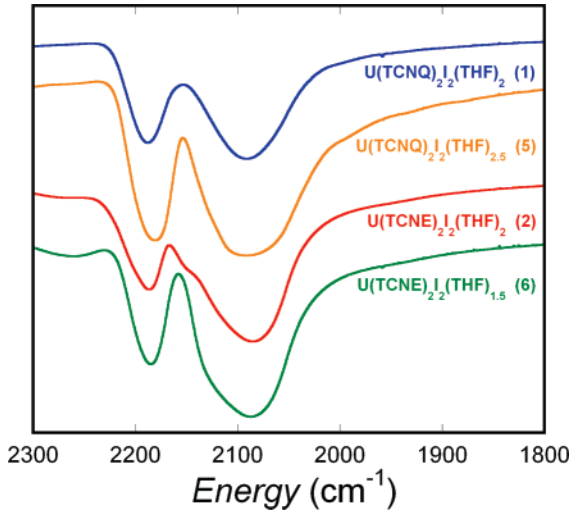

Figure 3. $\nu_{C\equiv N}$ Stretching region from the IR spectra of **1**, **2**, **5**, and **6**.

and suggest that $[U(TCNQ)_2I_2(THF)_2]_n$ (**1**) and $[U(TCNE)_2I_2(THF)_2]_n$ (**2**) are the accurate formulas for the compounds. In both cases, iodide ions balance the charge of the tetravalent uranium ions. The low nitrogen result for the C, H, N analysis for **2**, observed over several measurements, is consistent with reported difficulties in obtaining precise nitrogen analysis for metal−TCNX materials.[7,11]

In a similar manner, the reduced organic acceptor salts **3** and **4** react with $UI_3(THF)_4$ in THF to produce **5** and **6**, respectively (eq 2). Repeated measurements indicate the

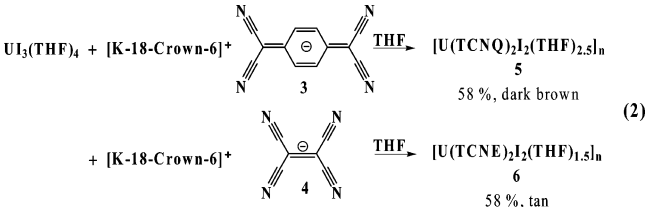

(2)

materials consistently analyze for **5** and **6**, though complex **6** is sensitive to desolvation, which is reflected in the lower precision of its elemental analysis. The fingerprint regions of the IR spectra for **5** and **6** differ from **1** and **2**, respectively, while the $\nu_{C\equiv N}$ regions are very similar to those observed for **1** and **2**, confirming the presence of $TCNX^{\bullet-}$ in **5** and **6** (Figure 3). Despite using the THF-soluble $TCNX^{\bullet-}$ starting materials, both products contain U(IV) rather than U(III) ions. The source of oxidizing agent for U(III) in eq 2 is unclear. The moderate yields of **5** and **6** could imply involvement of $TCNX^{\bullet-}$ as an oxidizing agent, though the final destination of reducing equivalent is unknown in the face of the several redox-active species present in the reaction mixtures. Compounds **1**, **2**, **5**, and **6** are all air-sensitive and discolor over minutes when removed from an inert atmosphere and exposed to air.

Structure of 4. Although **3** is known,[25,33−35] **4** has only been generated in solution for electron spin resonance studies

(30) *SHELXTL 5.10*; Bruker AXS, Inc.: Madison, WI, 1997.
(31) Zhang, J.; Ensling, J.; Ksenofontov, V.; Gutlich, P.; Epstein, A. J.; Miller, J. S. *Angew. Chem., Int. Ed. Engl.* **1998**, *37*, 657.
(32) Vickers, E. B.; Selby, T. D.; Thorum, M. S.; Taliaferro, M. L.; Miller, J. S. *Inorg. Chem.* **2004**, 43.
(33) Nogami, T.; Morinaga, M.; Kanda, Y.; Mikawa, H. *Chem. Lett.* **1979**, *1*, 111.
(34) Nogami, T.; Morinaga, M.; Mikawa, H.; Nakano, H.; Horioka, M.; Horiuchi, H.; Tokonami, M. *Bull. Chem. Soc. Jpn.* **1990**, *63*, 2414.

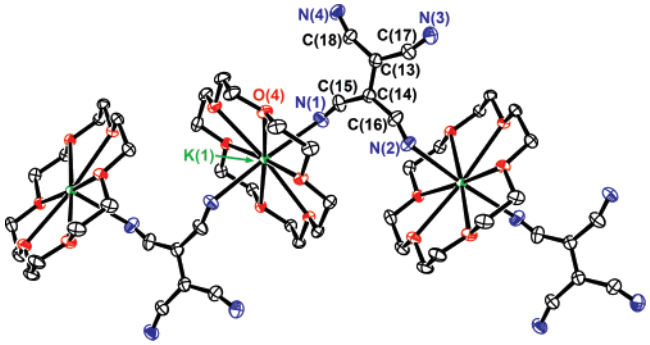

Figure 4. Thermal ellipsoid plot of **4** showing the 1D chain structure and 1,1-(*N*,*N*′)-TCNE linking mode. Ellipsoids are projected at the 30% probability level. The asymmetric unit of **4** consists of one $TCNE^{\bullet-}$ anion linked to a $[K\text{-18-crown-6}]^+$ complex cation.

and has not been isolated or characterized crystallographically.[36,37] Crystals suitable for single-crystal X-ray analysis of **4** were grown from a concentrated acetonitrile solution at −30 °C. As shown in Figure 4, compound **4** crystallizes in the expected ratio of one potassium ion (complexed by the crown ether), to one $TCNE^{\bullet-}$ radical anion. The structure of **4** displays a one-dimensional chain of complexed potassium cations linked by the $TCNE^{\bullet-}$ through nitrogen−potassium interactions. Interestingly, the chain is formed by 1,1-(*N*,*N*′)-TCNE bridging units instead of the more commonly observed 1,2-(*N*,*N*′)-TCNE linkage. This is illustrated in Figure 4 by the linkages through atoms N(1) and N(2) to potassium ions, rather than N(1) and N(3). Only one other structure is reported to exhibit the 1,1-TCNE linkage type.[38] The closest TCNE−TCNE interchain distances are greater than 8 Å, implying the radicals should exhibit isolated $S = 1/2$ magnetic behavior, which is consistent with the magnetic response for **4** at high temperatures (Supporting Information).

The $TCNE^{\bullet-}$ anions in **4** exhibit a 1:1-type disorder at atoms C(13) and C(14), which renders careful analysis of the geometric parameters of the anions problematic (Supporting Information). Nevertheless, bond distances and angles are generally consistent with expectations for a bridging $TCNE^{\bullet-}$ anion. The C(13)−C(14) distance in **4** is 1.383(10) Å, which is comparable to the range of values reported for μ-$TCNE^{\bullet-}$ (1.395(7)−1.425(7) Å).[14] Similarly, the C−CN (C(13)−C(17) = 1.505(9) Å, C(13)−C(18) = 1.469(9) Å) and C−CNK (C(14)−C(15) = 1.432(8) Å, C(14)−C(16) = 1.490(8) Å) distances in **4** are slightly longer than those typically observed for μ-$TCNE^{\bullet-}$ (C−CN = 1.396(5)−1.430(5) Å, C−CNK = 1.392(5)−1.420(7) Å).[14]

Voltammetric Behavior of Polymer Precursors. Voltammetric data (both square-wave and cyclic) were collected for all the starting materials ($UI_3(THF)_4$, TCNQ, TCNE, **3**, and **4**) used in the preparation of the coordination polymers, as well as for $[Bu_4N][I]$ in ∼0.1 M $[Bu_4N][B(C_6F_5)_4]$/THF to assess the properties of these redox-reactive species under conditions similar to those employed in the syntheses. Typical voltammetric data are presented for the neutral TCNX species in Figure 1 and for $UI_3(THF)_4$ and $[Bu_4N][I]$ in Figure 2. A complete summary of the thermodynamic redox values for these components and an indication of their heterogeneous electron-transfer kinetic properties are provided in Table 1.

Table 1. Summary of Redox Properties of Components of U(IV)/TCNX Coordination Polymers in 0.1 M $[Bu_4N][B(C_6F_5)_4]$/THF

	$E_{1/2}$[a] (V vs $[(C_5H_5)_2Fe]^{+/0}$)		
	at glassy carbon	at platinum	comment[b]
	"Oxidants"		
$TCNQ^{0/1-}$	−0.34	−0.33	reversible at both
$TCNQ^{1-/2-}$	−1.01	−1.00	reversible at both
$TCNE^{0/1-}$	−0.33	−0.35	reversible at GC, quasi-reversible at Pt
$TCNE^{1-/2-}$	−1.40	−1.69	quasi-reversible at GC, irreversible at Pt
$\mathbf{3}^{0/1-}$		−0.34	reversible
$\mathbf{3}^{1-/2-}$		−1.04	quasi-reversible
$\mathbf{4}^{0/1-}$		−0.33	quasi-reversible
$\mathbf{4}^{1-/2-}$		−1.62	irreversible
	"Reductants"		
$U^{IV/III}I_3(THF)_4$	−0.62		reversible
I_3^-/I^-	∼ −0.7		see text[c]

[a] Determined from peak position in square-wave voltammograms. [b] Reversibility criteria refer to standard electrochemical nomenclature,[41] and are based on cyclic voltammetric data. [c] Half-wave potential estimated from average of cathodic and anodic cyclic voltammetric peaks for couple in $[Bu_4N][I]$.

Our results are in excellent agreement with those published previously for TCNX systems in acetonitrile[39] and mixed THF/acetonitrile solution.[40] Specifically, both neutral organic acceptor ligands can be reduced in two sequential one-electron steps (Figure 1). The potential for the first reduction to generate the radical anion, $TCNX^{\bullet-}$, is nearly identical for both ligands. The second reduction process occurs at significantly more negative potentials for TCNE than it does for TCNQ. This second step is reported to generate the dianion species, $TCNX^{2-}$, instead of the diradical species for both ligands,[39] although the voltammetric data alone are insufficient to distinguish the two possibilities. The differences in the electron-transfer kinetic behavior for the two ligands and as a function of the working electrode substrate seen in our work have also been observed in acetonitrile solution.[39] The second reduction step for TCNE is in general more sluggish than the first reduction step and becomes irreversible at a platinum electrode in 0.1 M $[Bu_4N][B(C_6F_5)_4]$/THF. The data for the chemically prepared radical anions, **3** and **4**, are comparable to those for the neutral precursors (Table 1) in terms of the redox potentials, although these species in general exhibit more sluggish kinetic behavior than the corresponding neutral species, presumably reflecting the influence of the $[K\text{-18-crown-6}]^+$ ion-pairing

(35) Grossel, M. C.; Evans, F. A.; Hriljac, J. A.; Morton, J. R.; Lepage, Y.; Preston, K. F.; Sutcliffe, L. H.; Williams, A. J. *J. Chem. Soc., Chem. Commun.* **1990**, 439.
(36) Eastman, M. P.; Ramirez, D. A.; Jaeger, C. D.; Watts, M. T. *J. Phys. Chem.* **1976**, *80*, 182.
(37) Eastman, M. P.; Chiang, Y.; Bruno, G. V.; McGuyer, C. A. *J. Phys. Chem.* **1977**, *81*, 1928.
(38) Cotton, F. A.; Kim, Y.; Lu, J. *Inorg. Chim. Acta* **1994**, *221*, 1.
(39) Khoo, S. B.; Foley, J. K.; Pons, S. *J. Electroanal. Chem.* **1986**, *215*, 273.
(40) Kamau, G. N.; Rusling, J. F. *J. Electroanal. Chem.* **1990**, *292*, 187.
(41) Bard, A. J.; Faulkner, L. R. *Electrochemical Methods: Fundamentals and Applications*; John Wiley and Sons: New York, 2001.

Table 2. Summary of Characteristic Bands from the Infrared Spectra of **1**−**6** and Related Compounds

compound	$\nu_{C\equiv N}$ (cm^{-1})	$\nu_{C=C}$ (cm^{-1})	$\nu_{C-H(bend)}$ (cm^{-1})	ref
TCNQ	2222 m	1542 m	858 m	15
[K-18-crown-6][TCNQ] (**3**)	2186 s, 2176 s, 2160 sh, 2155 s	1504 s	843 sh, 838 m, 833 m	this work
$[U(TCNQ)_2I_2(THF)_2]_n$ (**1**)	2188 s, 2091 s	1506 m	851 w, 824 w, 808 w	this work
$[U(TCNQ)_2I(THF)_{2.5}]_n$ (**5**)	2181 s, 2091 s	1508 s	840 w, 824 m	this work
$[Gd_2(TCNQ)_5(H_2O)_9][Gd(TCNQ)_4(H_2O)_3]$	2177 s	[a]	[a]	12
$V(TCNQ)_2 \cdot (CH_2Cl_2)_{0.84}$	2190 s, 2088 s, 2024 sh	[a]	[a]	32
$Mn(TCNQ)_2$	2205 s, 2187 s, 2137 sh	1505 s	826 m	7
$Fe(TCNQ)_2$	2217 s, 2187 s, 2142 sh	1505 s	827 m	7
$Co(TCNQ)_2$	2217 s, 2188 s, 2137 sh	1505 s	827 m	7
$Ni(TCNQ)_2$	2224 s, 2208 s, 2192 s, 2155 sh	1503 s	829 m	7
TCNE	2262 s, 2228 m, 2214 w	1570 (Raman)		14
[K-18-crown-6][TCNE] (**4**)	2191 s, 2153 s, 2140 sh	[b]		this work
$[U(TCNE)_2I_2(THF)_2]_n$ (**2**)	2187 s, 2149 sh, 2085 s	[b]		this work
$[U(TCNE)_2I_2(THF)_{1.5}]_n$ (**6**)	2185 s, 2087 s	[b]		this work
$Gd(TCNE)_3$	2219 m, 2181 s, 2154 s	[a]		16
$Dy(TCNE)_3$	2220 m, 2182 s, 2156 s	[a]		16
$V(TCNE)_2$	2188 s, 2099 s	[a]		10
$Mn(TCNE)_2$	2280 vw, 2224 m, 2181 s, 2171 s	[a]		31
$Fe(TCNE)_2$	2279 vw, 2221, m, 2177 s, 2174 s	[a]		31
$Co(TCNE)_2$	2284 vw, 2230 m, 2187 s, 2167 s	[a]		31
$Ni(TCNE)_2$	2290 vw, 2237 m, 2194 s	[a]		31

[a] Not reported. [b] Not observed. Sample prepared using Nujol mull.

(see Supporting Information). Similar strong influences on charge-transfer kinetics with changing supporting electrolyte composition have been attributed to such ion-pair effects.[39]

The voltammetric response observed for $UI_3(THF)_4$ indicates a reversible oxidation of the metal center and, at more positive potentials, an irreversible wave of significantly greater current amplitude that is attributed to the oxidation of coordinated iodide ligands (Figure 2). The current in this irreversible wave from square-wave scans is approximately three times that of the metal-based wave, suggesting that all three bound I^- ligands are oxidized. As shown in Figure 2 (top panel), if the voltammetric scans proceed into the potential range of this latter process, the metal-based reduction component is no longer observed consistent with decomposition of the UI_3 species due to iodide oxidation.

To assess the difference in redox behavior of metal-bound versus free iodide ion, data were also collected for a $[Bu_4N][I]$ solution. The voltammetric behavior of the iodide ion under these conditions (Figure 2, bottom panel) is complicated, but in general consistent with that reported previously for iodide ion in aprotic solvent.[42] The first (most negative) oxidation wave is attributed to the oxidation of I^- to I_3^-, and the second oxidation wave is assigned to oxidation of I_3^- formed in the first wave to I_2.[42] Note that when the cyclic scan is reversed immediately after the first oxidation wave, a corresponding reduction wave attributed to the reverse process (I_3^- to I^-) is observed. When scans proceed into the second oxidation wave, this reduction wave occurs at the same potential but increases in amplitude. This increase in current can be attributed to the formation of additional I_3^- after the second oxidation wave as a result of the strong association of bulk I^- with I_2 to form I_3^- in a non-redox reaction.[43] While a stringent thermodynamic value for the formal redox potential of neither of the couples evidenced in these data is possible on the basis of the voltammetric data, the existence of both anodic and cathodic waves for the I_3^-/I^- couple allows a rough estimate of the $E_{1/2}$ value for this process as the average of anodic and cathodic peak potentials, as indicated in Table 1. This provides some assessment of the relative reducing capability of the iodide ion under the conditions employed. It is also noteworthy that the potential region for the iodide oxidation process(es) in $UI_3(THF)_4$ is comparable to that for free I^-, as illustrated in Figure 2 (bottom panel).

On the basis of the voltammetric data described above, either of the potential reductants in the polymer synthesis reactions, U(III) or I^-, has sufficient thermodynamic driving force to reduce either TCNX acceptor ligand by one electron to the radical anion state. In fact, we confirmed in our system that mixing of THF solutions of $[Bu_4N][I]$ and neutral TCNX immediately produced the characteristic colors of the radical anion species, orange-yellow for $TCNE^{\bullet -}$ and emerald green for $TCNQ^{\bullet -}$, and subsequent voltammetry confirmed that the solution rest potentials moved between the two redox waves illustrated in Figure 1.

Infrared Spectroscopy. Infrared spectra for complexes **1**−**6** were recorded as Nujol mulls. Table 2 lists the observed band energies for **1**−**6** in addition to reported values from the literature for related compounds. Of interest in the spectra of the TCNQ complexes is the $\nu_{C\equiv N}$ stretching region from ∼2000 to 2300 cm^{-1}, the $\nu_{C=C}$ stretching mode at ∼1500−1550 cm^{-1}, and the ν_{C-H} bending mode at ∼800−865 cm^{-1}.[2,7,12,44] Comparison with the data for neutral TCNQ indicates that TCNQ is present in a reduced form for compounds **1** and **5**, as noted by the shifts of the nitrile frequencies to lower energies (from 2262 and 2228 to 2181 and 2091 cm^{-1} for **1**), the $\nu_{C=C}$ stretches at ∼1506 and 1508 cm^{-1} for **1** and **5** and the ν_{C-H} bending energies from 808−851 cm^{-1}.[2,7,13] While low, the energies of the two strong $\nu_{C\equiv N}$ stretching bands observed for **1** are very similar to those

(42) Popov, A. I.; Geske, D. H. *J. Am. Chem. Soc.* **1958**, *80*, 1340.
(43) Wang, X.; Stanbury, D. M. *Inorg. Chem.* **2006**, *45*, 3415.
(44) Bartley, S. L.; Bazile, M. J., Jr.; Clerac, R.; Zhao, H.; Ouyang, X.; Dunbar, K. R. *Dalton Trans.* **2003**, 2937.

reported for $V(TCNX)_2$,[10,32] and their broadness indicates that the TCNQ ligands possess multiple coordination environments (Figure 3). The $\nu_{C\equiv N}$ band energies roughly provide general information on the extent of reduction of TCNQ (> ~2220 cm^{-1}), $TCNQ^{\bullet-}$ (~2100−2220 cm^{-1}) or $TCNQ^{2-}$ (< ~2100 cm^{-1}),[15] with the caveat that σ-bonding interactions of the nitrile groups shift these modes to higher energies, while metal-to-nitrile π-back-donation shifts them to lower energies.[15] For the uranium−nitrile metal−ligand interactions in the materials reported here, the effect of nitrile coordination is primarily of a σ-type, as judged by comparison of the nitrile absorbances for $UCl_4(N\equiv CCH_3)_4$ (2278 cm^{-1}) versus free acetonitrile (2249 cm^{-1}).[45] The nitrile band energies for **1**, **2**, **5**, and **6** confirm the presence of $TCNX^{\bullet-}$ in these materials (Table 2). Furthermore, the similarities of the energies of these bands between **1** and **5** and **2** and **6** demonstrates the presence of the U(IV) ion in all these materials.

Further structural information is garnered through examination of the C−H bending regions for the TCNQ materials.[7] For example, compound **1** exhibits a characteristic C−H bending mode at 808 cm^{-1}, a value definitive for indication of the presence of σ-dimerized $[TCNQ-TCNQ]^{2-}$.[7,13] The second C−H bending band at 824 cm^{-1} is consistent with $TCNQ^{\bullet-}$.[13] The bending band for **1** at 851 cm^{-1} is consistent with partially oxidized $TCNQ^{\bullet-}$, lying intermediate between a fully reduced signature (~826−831 cm^{-1}) and neutral TCNQ (~861 cm^{-1}).[46] As such, the observed simple stoichiometry of **1** belies a structural complexity indicated by the C−H bending region of its infrared spectrum. The complexity of the structure of **1** is comparable to the single reported polymeric f-element−TCNQ structure, Gd(III)−TCNQ, which consists of TCNQ in multiple coordination modes forming interpenetrated anionic and cationic metal−TCNQ lattices.[12]

As mentioned above, comparison of the IR data for **1** with **5** reveals a similar number and energy of nitrile stretching bands. However, the C−H region of compound **5** exhibits only one strong and one weak band, consistent with fully reduced and partially oxidized TCNQ, respectively. Despite their similar stoichiometries, the differences in energies and number of bands in the C−H region suggest that **1** and **5** comprise distinct polymeric phases. This is consistent with the different colors observed for these materials. Similarly, the nitrile stretching energies for **2**, **4**, and **6** indicate reduced TCNE in all three materials. The comparable number and energies of the $\nu_{C\equiv N}$ stretching bands for **2** and **6** also indicate that $TCNE^{\bullet-}$ is present in both compounds. Characteristic $\nu_{C=C}$ stretches were not observed for these materials.[14]

Magnetism. The magnetic susceptibility responses of $UI_3(THF)_4$ and compounds **1**, **2**, **5**, and **6** are shown in Figure 5, and field-dependent magnetization data are shown in Figure 6. It is instructive to compare the magnetic behavior of the coordination polymers **1**, **2**, **5**, and **6** with that of the simple U(III) complex, $UI_3(THF)_4$. Analysis of the sum of the magnetic behaviors for **1**, **2**, **5**, and **6**, especially their magnetic moments and absence of magnetic ordering, affords general conclusions on the gross magnetic structures in these materials. The magnetic data for the compounds immediately reveal that the behaviors of **1**, **2**, **5**, and **6** are all similar to one another, while the trivalent $UI_3(THF)_4$ exhibits significantly different behavior. Importantly, compounds **1**, **2**, **5**, and **6** all show behavior consistent with the presence of a U(IV) ion.

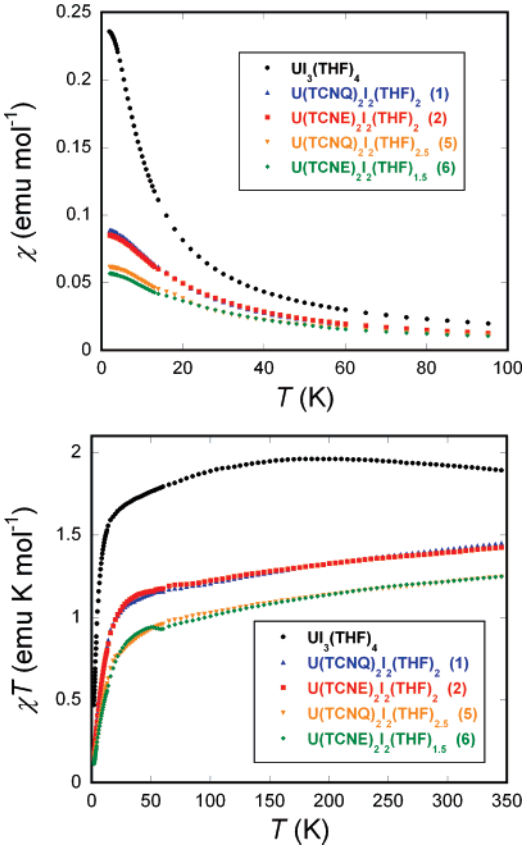

Figure 5. Temperature-dependent magnetic susceptibility data for $UI_3(THF)_4$, **1**, **2**, **5**, and **6** in the range of 1.8−350 K.

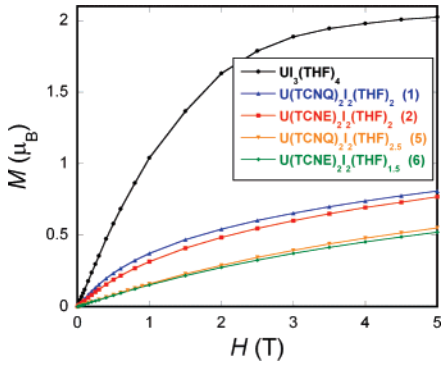

Figure 6. Field-dependent magnetization data for $UI_3(THF)_4$, **1**, **2**, **5**, and **6** collected at 2 K. Lines are a guide for the eye.

The electronic structure of the $5f^2$ U(IV) ion is dominated by electron−electron repulsions and spin−orbit coupling such that the ground term for this ion is usually approximated as $^3H_4$ using the $L-S$ coupling scheme.[47] Low-symmetry ligand fields acting on the $J = 4$ term completely lift its

(45) Bagnall, K. W.; Brown, D.; Jones, P. J. *J. Chem. Soc. A: Inorg., Phys., Theo.* **1966**, 1763.
(46) Pukacki, W.; Pawlak, M.; Graja, A.; Lequan, M.; Lequan, R. M. *Inorg. Chem.* **1987**, *26*, 1328.

degeneracy yielding $2J + 1 = 9$ ligand-field levels. The predicted high-temperature value for population of all nine ligand-field states of the U(IV) ion is ($S = 1$, $L = 5$, $J = 4$, $g = 0.8$) 1.60 emu K mol^{-1} (3.58 μ_B). In general, most molecular U(IV) complexes have ligand-field splittings larger than the thermal energy at $kT = 300$ K and a ground-state magnetic singlet term from these nine states such that their low-temperature magnetic response becomes temperature independent.[47] The low-temperature response of such ions achieves a constant value in the χ vs T data. Residual paramagnetism observed at low temperatures is due to Van Vleck temperature-independent paramagnetism (TIP) of the first excited-state mixing into the ground ligand-field state. Thermal Boltzmann population of the first excited state (often $\sim$200 cm^{-1} above the ground state) gives rise to the observed high-temperature magnetic moment (often ranging from $\sim$0.7 to 1.2 emu K mol^{-1}),[47] the result of contributions from only a few of the lowest lying ligand-field states yielding orbital magnetism.

Compounds **1**, **2**, **5**, and **6** exhibit high-temperature χT values from 1.25 to 1.46 emu K mol^{-1}. At this high-temperature limit the compounds are expected to behave as magnetically isolated spin centers. As such, the predicted contributions from the organic radicals should be $2 \times 0.375 = 0.750$ emu K mol^{-1} (the Curie value for two isolated $S = 1/2$ spin centers). This condition places lower limit values of the contribution of the U(IV) ions of **1**, 0.71 **2**, 0.68; **5**, 0.50; and **6**, 0.50 emu K mol^{-1} at 350 K. These values are lower than those typically observed for U(IV) complexes,[22,47,48] perhaps indicating σ- or π-dimerization of TCNX in these materials, which would attenuate the contribution of the two organic radicals per empirical formula unit at high temperatures. This contention is supported by the observation of the $\nu_{C-H\ (bend)}$ signature for [TCNQ$-$TCNQ]$^{2-}$ in **1**. As expected, the approximate χT product values for the U(IV) ions indicate that the ligand-field splittings in these compounds are larger than the thermal energy kT in the high-temperature limit of this experiment.

The χ vs T data for **1**, **2**, **5**, and **6** increase with decreasing temperatures then level off and achieve constant values. This low-T behavior is consistent with a contribution dominated by the U(IV) ion. The dominance of the U(IV) signal is further evidence for reduction of the contribution of the two $S = 1/2$ TCNX$^{\bullet-}$ spin centers (from the formula units assigned above) from significant portions of dimerized (σ and/or π) TCNX units in these materials. This is also evidence for a more complex structure of the materials than indicated by their simple empirical formulae. The χT vs T data decrease with temperature and approach the expected value of zero at low temperatures (Figure 5) from the primary U(IV) signature.

The magnetic singlet ground state of U(IV) observed for **1**, **2**, **5**, and **6** is easily contrasted with the $^4I_{9/2}$ ground term from the $5f^3$ configuration of the U(III) ion at low temperatures.[49] Trivalent uranium possesses a ground Kramer's doublet such that the χ vs T response for U(III) ions will continue to increase at low temperatures, which is the behavior observed for $UI_3(THF)_4$ (Figure 5). The high-temperature value observed for this compound 1.89 emu K mol^{-1} is comparable to reported values for the U(III) ion.[49] The strong temperature dependent decrease of the χT product indicates a large ligand-field splitting of this ion. Although the calculated Curie values for U(III) (3.62 μ_B) and U(IV) (3.58 μ_B) ions are similar, the low-symmetry ligand field present in $UI_3(THF)_4$, **1**, **2**, **5**, and **6** allows for differentiation between the ions from the magnitude of their magnetic susceptibility responses. The differences between the ions are further highlighted in the field-dependent magnetization data for the compounds collected at 2 K (Figure 6). The compounds **1**, **2**, **5**, and **6** all show a small response of <0.5 μ_B typical for the singlet ground state with residual paramagnetism from state mixing for the U(IV) ion (and presumable some fraction of undimerized TCNX$^{\bullet-}$), while $UI_3(THF)_4$ has a much larger response consistent with a ground state possessing a first-order Zeeman effect. The sum total of the magnetic data provide clear indication that compounds **1**, **2**, **5**, and **6** contain only U(IV) ions. AC susceptibility experiments performed on them at 1000 Hz in $H = 0$ with a 3 Oe driving field from 100 to 2 K reveal that none of the compounds undergo magnetic ordering. The lack of magnetic ordering in **1**, **2**, **5**, and **6** is presumably due to the singlet magnetic ground state of the U(IV) ion, similarly noted for the three-dimensional oxalate material $K_2MnU(C_2O_4)_4 \cdot 9H_2O$.[50]

Conclusions

Reactions of $UI_3(THF)_4$ with both neutral and reduced organic acceptors TCNE and TCNQ yield coordination polymers. In all cases the materials exhibit $\nu_{C\equiv N}$ stretching frequencies consistent with reduced TCNX$^{\bullet-}$ organic acceptors. Starting with neutral TCNX precursors, the reactions with $UI_3(THF)_4$ result in metal oxidation producing coordination polymers of U(IV) that exhibit a ligand-field magnetic singlet ground state. These materials do not exhibit magnetic ordering, presumably due to the presence of the U(IV) ion and/or the presence of σ- or π-dimerized organic acceptors. Efforts to preserve the U(III) ion in the resulting material with the use of reduced TCNX$^{\bullet-}$ starting materials also yielded materials consistent with tetravalent uranium, evidenced by $\nu_{C\equiv N}$ stretching modes, voltammetric data, temperature-dependent susceptibility, and low-temperature magnetization data, though the fate of the chemical oxidizing agent in these reactions remains unclear. The ultimate production of a uranium molecular magnet will require pairing with a suitable organic acceptor that maintains the uranium ion in an oxidation state exhibiting a magnetic Kramer's doublet ground state, which, on AF coupling, will be uncompensated by the organic spin.

(47) Boudreaux, E. A.; Mulay, L. N. *Theory and Applications of Molecular Paramagnetism*; Wiley: New York, 1976; p 512.
(48) Kiplinger, J. L.; Pool, J. A.; Schelter, E. J.; Thompson, J. D.; Scott, B. L.; Morris, D. E. *Angew. Chem., Int. Ed.* **2006**, *45*, 2036.
(49) Castro-Rodriguez, I.; Meyer, K. *Chem. Commun.* **2006**, 1353.
(50) Moertl, K. P.; Sutter, J.-P.; Golhen, S.; Ouahab, L.; Kahn, O. *Inorg. Chem.* **2000**, *39*, 1626.

Acknowledgment. For financial support of this work, we acknowledge the LANL Glenn T. Seaborg Institute for Transactinium Science (Postdoctoral fellowship to E.J.S.), LANL (Director's Postdoctoral Fellowship to E.J.S.), the LANL Laboratory Directed Research and Development Program, and the Division of Chemical Sciences, Office of Basic Energy Sciences, Heavy Element Chemistry program. E.J.S. is the recipient of a Frederick Reines Postdoctoral Fellowship at Los Alamos. This work was carried out under the auspices of the National Nuclear Security Administration of the U.S. Department of Energy at Los Alamos National Laboratory under Contract No. DE-AC52-06NA25396. We thank Dr. Rico E. Del Sesto for helpful discussions in the preparation of this manuscript.

Supporting Information Available: CIF file, crystallographic details, and tables of bonds distances and angles for **4**; electrochemical data for **3** and **4**; and magnetic susceptibility data for **4**. This material is available free of charge via the Internet at http://pubs.acs.org.

IC0700295